

Research Paper

Use of FVB Myc-CaP cells as an immune competent, androgen receptor positive, mouse model of prostate cancer bone metastasis



Yu Wang^a, Mackenzie K. Herroon^{b,c}, Steven P. Zielske^c, Leigh Ellis^d, Izabela Podgorski^{b,c}, Russell S. Taichman^{a,e}, Frank C. Cackowski^{c,f,*}

^a Department of Periodontics and Oral Medicine, University of Michigan School of Dentistry, Ann Arbor, MI, USA

^b Department of Pharmacology, Wayne State University School of Medicine, Detroit, MI, USA

^c Department of Oncology, Wayne State University School of Medicine and Karmanos Cancer Institute, Detroit, MI, USA

^d Department of Medicine, Cedars-Sinai Medical Center, Los Angeles, CA, USA

^e Department of Periodontology, University of Alabama at Birmingham School of Dentistry, Birmingham, AL, USA

^f Department of Medicine, Division of Hematology, & Oncology, University of Michigan School of Medicine, Ann Arbor, MI, USA

ARTICLE INFO

Article history:

Received 24 May 2021

Revised 6 August 2021

Accepted 8 August 2021

Available online 18 August 2021

Keywords:

Prostate cancer

Metastasis

Bone

Model system

Androgen receptor

Immune competent

ABSTRACT

Prostate cancer (PCa) metastasis research has been hamstrung by lack of animal models that closely resemble the disease present in most patients – that metastasize to bone, are dependent on the androgen receptor (AR), and grow in an immune competent host. Here, we adapt the Myc-CaP cell line for use as a PCa androgen dependent, immune competent bone metastases model and characterize the metastases. After injection into the left cardiac ventricle of syngeneic FVB/NJ mice, these cells formed bone metastases in the majority of animals; easily visible on H&E sections and confirmed by immunohistochemistry for Ar and epithelial cell adhesion molecule. Mediastinal tumors were also observed. We also labeled Myc-CaP cells with tdTomato, and confirmed the presence of cancer cells in bone by flow cytometry. To adapt the model to a bone predominant metastasis pattern and further examine the bone phenotype, we labeled the cells with luciferase, injected in the tibia and observed tumor formation only in tibia with a mixed osteolytic/osteoblastic phenotype. The presence of Myc-CaP tumors significantly increased tibia bone volume as compared to sham injected controls. The osteoclast marker, TRAcP-5b was not significantly changed in plasma from tibial tumor bearing animals vs. sham animals. However, conditioned media from Myc-CaP cells stimulated osteoclast formation *in vitro* from FVB/NJ mouse bone marrow. Overall, Myc-CaP cells injected in the left ventricle or tibia of syngeneic mice recapitulate key aspects of human metastatic PCa.

© 2021 The Authors. Published by Elsevier GmbH. This is an open access article under the CC BY-NC-ND license (<http://creativecommons.org/licenses/by-nc-nd/4.0/>).

1. Introduction:

Prostate cancer (PCa) causes over 33,000 deaths per year in the United States [1]. However, there are relatively few models available to study its pathophysiology, especially for metastatic disease, and with characteristics that closely mimic the disease of most patients [2]. Genetically engineered mouse models of PCa have been developed based on expression of the SV40 large T antigen; (transgenic adenocarcinoma of the mouse prostate (TRAMP)), or deletion of *Pten* targeted to the prostate gland [3–5]. Xenograft models metastasize to bone and other tissues but lack a normal

immune system and are almost completely devoid of signaling downstream of the androgen receptor (AR) [6–8].

A basis for improvement in PCa mouse models came with the development of the Myc-CaP cell line [9]. This line was initially developed from a spontaneous prostate tumor of a c-myc overexpressing mouse and shows overexpression of wild type Ar [9] and also Ar splice variants [10]. Mammary fat pad tumors developed from this cell line partially regress after animals are castrated [9]. Additionally, because they are syngeneic, they have been used in studies of tumor immunology and immunotherapy when injected subcutaneously or as an intraosseous injection into the femur, but with minimal characterization of bone tumors formed after femur intraosseous injection [11–13]. However, adaptation of the FVB Myc-CaP cell line to model disseminated PCa has progressed at a slower pace. A recent report describes use of the cell line to induce liver tumors after injection in the spleen [14]. The same cell line on the C57BL/6 rather than the original FVB/NJ

* Corresponding author at: Wayne State University and Karmanos Cancer Institute, Department of Oncology, Room 715 Hudson Webber Cancer Research Center, Detroit, MI, USA.

E-mail address: cackowskif@karmanos.org (F.C. Cackowski).

background was recently shown to form bone tumors after systemic (intra-cardiac) inoculation, but only from a single cell suspension of an existing tumor – which limits the studies that can be performed with the model [15]. Here, we inject FVB Myc-CaP cells maintained under routine culture conditions in the left cardiac ventricle of syngeneic mice and observe metastases to multiple bones. To better study the bone phenotype of the cells, we directly injected the cells in the tibia of mice and observed formation of large mixed osteolytic/osteoblastic tumors and characterized their bone phenotype. Therefore, we expect these models to be invaluable for future studies of PCa bone metastases.

2. Materials and methods

2.1. Cell culture and *in vitro* assays

The Myc-CaP cell line on the FVB background (#CRL-3255) was obtained from ATCC and cultured as recommended in DMEM with 10% FCS. PC3 cells were obtained from ATCC (#CRL-1435) and cultured in RPMI with 10% FCS. Myc-CaP cells were labeled by lentiviral transduction with either; tdTomato (CloneTech Lenti-LVX-IRES) and selected by FACS, or labeled with firefly luciferase (Genecopoeia hLUC-Lv105) and selected with puromycin. To model mouse osteoclast (OCL) formation, bone marrow cells from FVB/NJ mice not adherent to tissue culture plastic were used as previously described [16]. The cells were cultured for 7 days in α -MEM with 10% FCS and 10 mg/ml of rhM-CSF (R&D Systems) and rhRANKL (R&D Systems) at a sub-maximal concentration of 10 ng/ml to allow for stimulation by added conditioned media (CM). 2×10^5 cells were seeded per well in 200 μ l volume in 96 well plates. Media was changed every other day. For conditioned media collection, 5×10^5 Myc-CaP or PC3 cells were seeded in 10 cm dishes in their usual growth media (DMEM or RPMI respectively) containing 10% FCS and cultured for one day. For CM collection, the media was changed to α -MEM with 10% FCS and cells were cultured for an additional day prior to CM collection. CM was added to OCL cultures at 25% of the total volume (50 μ l per well). Cultures were fixed with 10% neutral buffered formalin, and stained for tartrate resistant acid phosphate (TRAP/Acp5) as previously described [17]. TRAP⁺ cells with three or more nuclei were counted as OCLs. To assay TRAP activity secreted into culture media, 100 μ l of media collected after 5 days of culture was combined with 200 μ l of TRAP substrate and absorbance at 562 nm was determined with a microplate reader [17]. Bone resorption and formation markers were evaluated by ELISA of plasma samples; TRAP-5b (Immunodiagnostic Systems #SB-TR103), type 1 collagen pro-peptide (Immunodiagnostic Systems #AC-33F1) and osteocalcin (Novus Biologicals #NBP2-68151). Osteoclastogenic factors were measured from conditioned media of Myc-CaP cells; soluble Rankl (R&D Systems #MTR00) and Cxcl15/Il-8 (RayBiotech #ELM-CXCL15).

2.2. Animal models and imaging

All studies were approved by the Institutional Animal Care and Use Committee of the University of Michigan. 5×10^5 or 5×10^4 cells recovered from *in vitro* culture were injected in the cardiac left ventricle or left tibia respectively of male syngeneic FVB/NJ mice (Jackson Labs) as previously described [18]. Bioluminescence *in vivo* imaging or fluorescence *ex vivo* imaging were conducted with a Perkin Elmer IVIS 2000 instrument. For bioluminescence imaging, 200 mg/kg of Promega VivoGloTM luciferin was injected 10 min prior to imaging under 2% isoflurane in oxygen anesthesia. Mice were euthanized by CO₂ asphyxiation if they became moribund from disease, had tumors > 1 cm, were not using the affected leg, or at experiment endpoint. After euthanasia, blood was col-

lected into EDTA tubes and centrifuged to collect plasma. Tissues were drop fixed in 10% neutral buffered formalin for one day at 4 °C and then stored in 70% ethanol. Bone specimens were imaged with a microCT system (μ CT100, Scanco Medical, Bassersdorf, Switzerland). Scan settings were: voxel size 12 μ m, 70 kVp, 114 μ A, 0.5 mm AL filter, and integration time 500 ms. Analysis was performed using the manufacturer's evaluation software, and a fixed global threshold of 18% (180 on a grayscale of 0–1000) was used to segment bone from non-bone. A 6 mm region of bone was analyzed beginning immediately below the growth plate for 500 slices. Bone volume and tissue mineral density were generated and compared with the control tibiae for each animal.

2.3. Histology and immunohistochemistry

Bones were then decalcified in multiple changes of 10% EDTA pH 8 for 3 weeks at 4 °C and embedded in paraffin. 5 μ m sections stained with hematoxylin and eosin were used for general morphologic assessment. Blue staining on Masson's Trichrome was used to assess collagen. TRAP (Acp5) cytochemistry was used to visualize OCLs, followed by hematoxylin counterstaining and aqueous mounting as described [17]. PCa origin of tumors was confirmed by immunohistochemistry. After de-waxing and permeabilization with PBS with 0.1% Triton X-100 (PBT), immunohistochemistry (IHC) conditions were as follows: For Ar and Epcam; antigen retrieval was performed with pepsin (Invitrogen #003009) for 15 min at 37 °C. Endogenous peroxidases were blocked with 3% hydrogen peroxide in PBS for 15 min at room temperature. Slides were blocked with 5% goat serum in PBT overnight at 4 °C. Primary antibodies for androgen receptor (Millipore antibody #06-680, diluted 1:50) and Epcam (Abcam antibody #71916, diluted 1:250) or the corresponding concentrations of rabbit IgG were diluted in PBT and applied at room temperature for one hour. Slides were washed with PBT and visualized using reagents provided with the Vector rabbit ABC EliteTM kit (#PK-6101). Slides were subsequently counterstained with hematoxylin, dehydrated and mounted. For F4/80, antigen retrieval was with 10 mM pH 6 sodium citrate with 0.05% tween heated to 125 °C for 30 s, then 90 °C for 10 s at 15 psi in a Biocare medical DC2002 Decloaking Chamber. The primary antibody was a monoclonal rabbit anti-mouse (Cell Signaling Technology #99940) diluted 1:200. For Cd3 ϵ , antigen retrieval was with Antigen Unmasking Solution Tris pH 9 (Vector Labs #H-3301) heated in a pressure cooker as above and the primary antibody was monoclonal rabbit anti-mouse diluted 1:100 (Cell Signaling Technology #99940). For F4/80, and Cd3 ϵ , peroxidase staining was with the Vector Laboratories NovaRED kit (#SK-4805).

2.4. FACS and flow cytometric analysis

All analyses were conducted on a BD FACS AriaIIu cell sorter and analyzer with 405 nm, 488 nm, and 630 nm lasers and non-linear detectors. After transduction, successive rounds of FACS for tdTomato (PE channel) were performed until a uniform population was obtained. Unlabeled Myc-CaP cells were used as a negative control. To detect tdTomato positive tumor cells *in vivo*, lungs or bones (tibia, femur and lumbar vertebrae) were disrupted with a mortar and pestle and strained. The cells were labeled with DAPI and mouse PE/Cy7 conjugated Ter119 (Biolegend #116222) and APC conjugated Cd45 (Biolegend #103112) antibodies. Putative tumor cells were defined as single viable cells, negative for Ter119, and successively negative for Cd45 but positive for tdTomato.

2.5. Statistical analyses

Student's unpaired equal variance *t*-test was used to compare two means. Multiple means were analyzed with one-way ANOVA with Tukey post-hoc testing. The log-rank test was used for survival analyses. All analyses were conducted with GraphPad Prism software.

3. Results

We injected half a million Myc-CaP cells into the left cardiac ventricle of eight FVB/NJ mice and injected 4 mice with phosphate

buffered saline (PBS) as sham controls. The animals injected with Myc-CaP cells died or were moribund at a median of 30 days after injection (Fig. 1A). Upon necropsy of these animals, with the aid of H&E histology, we observed tumors in bones of 4 of 7 animals and in the chest of all 7 animals analyzed (Fig. 1B). One animal was not analyzed by histology due to inadequate preservation of the specimen. We did not observe tumors in the kidneys, livers, gastrointestinal tracts, or genitourinary tracts by gross analysis or H&E histology. We confirmed the presence of bone metastases by immunohistochemistry (IHC) for both androgen receptor and epithelial cell adhesion molecule (EPCAM) (Fig. 1C). At the level of gross anatomic analysis, the tumors in the chest cavities,

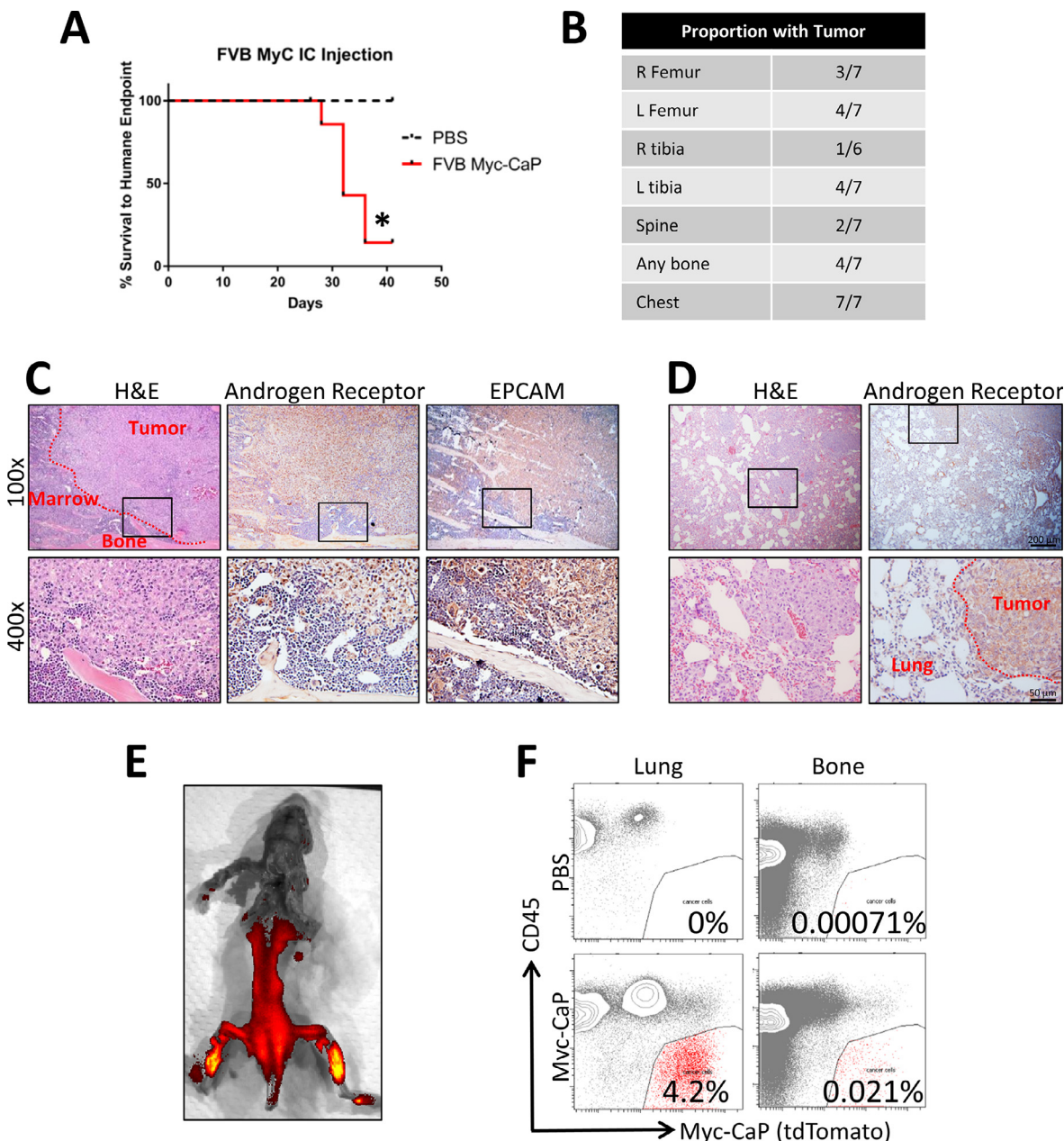


Fig. 1. Distribution of tumors formed by FVB Myc-CaP cells after left ventricle injection by gross analysis, histology, fluorescence imaging, and flow cytometry. (A) Kaplan-Meier curve of time to death or humane endpoint of FVB mice injected with parental FVB Myc-CaP cells (*n* = 8) or PBS as a negative control (*n* = 4). * indicates *p* < 0.05 by the log rank test. (B) Number of animals injected with tumor cells with tumor visible on H&E sections at each listed anatomic site. (C) Immunohistochemical (IHC) validation of tumor identity of suspected bone metastases. Representative images for sections stained with H&E or IHC staining against either androgen receptor or Epcam (brown) with hematoxylin counterstain (blue). Original magnification 100x (10x objective), or 400x (40x objective). Area of higher magnification is indicated by the boxes. (D) IHC validation of tumor identity of suspected lung metastases. (E) *ex vivo* fluorescent imaging of the CNS and MSK systems of a mouse injected in the left ventricle with tdTomato labeled FVB Myc-CaP cells. (F) Flow cytometry plots showing detection of tumor cells at metastatic sites (lung or bone) from sham (PBS) or tumor injected animals. (For interpretation of the references to colour in this figure legend, the reader is referred to the web version of this article.)

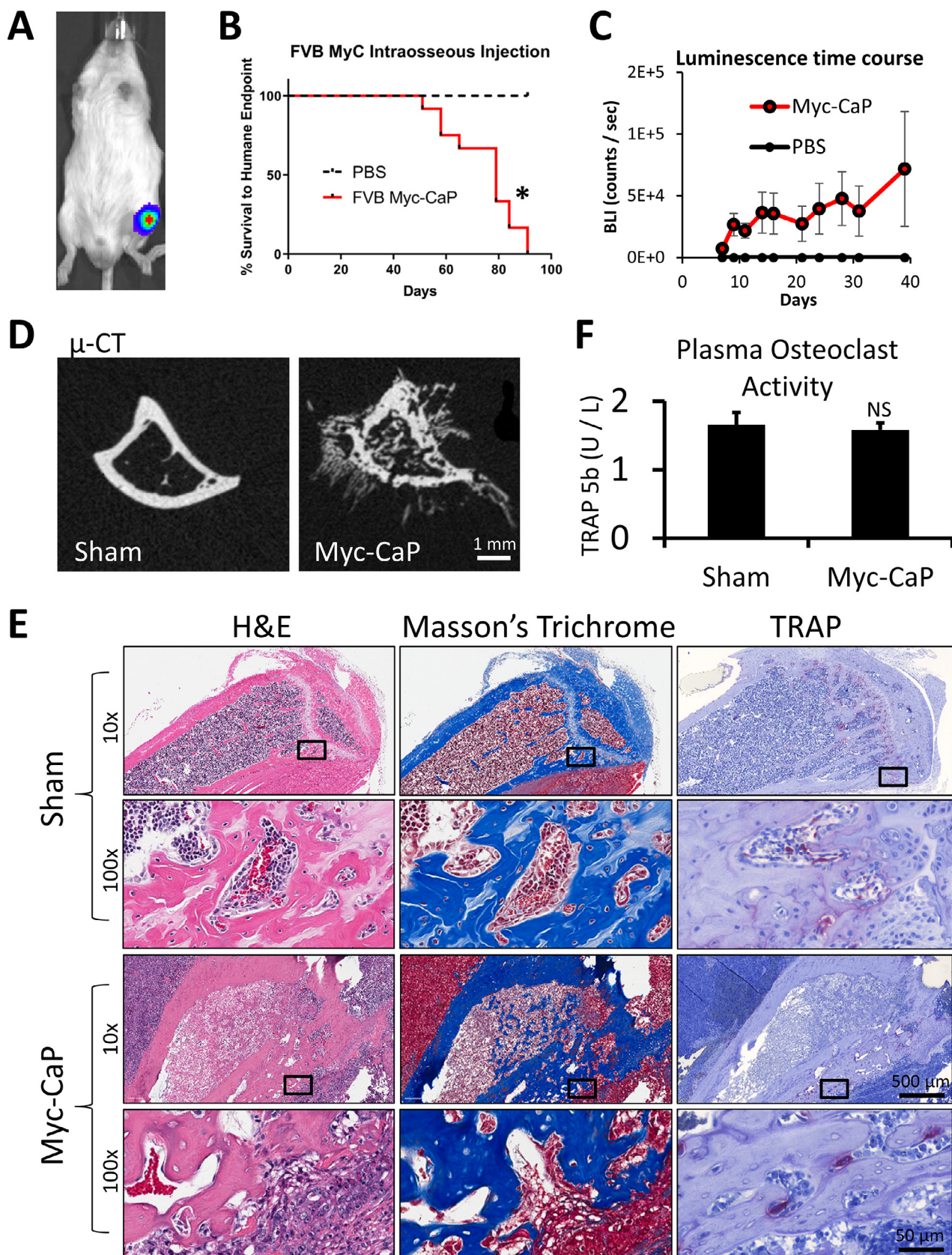


Fig. 2. Myc-CaP tumor formation after intra-tibial injection. (A) Example bioluminescence image of mouse injected with luciferase labeled Myc-CaP cells. (B) Kaplan-Meier curve of time to humane endpoint of FVB mice injected with parental FVB Myc-CaP cells ($n = 14$) or PBS ($n = 4$) as a negative control. (C) Mean bioluminescence \pm SEM over time of Myc-CaP or PBS (sham) tumors. (D) Sample axial micro-CT images of tibia injected with PBS or Myc-CaP cells. (E) Sample sections stained with hematoxylin and eosin (left), Masson's trichrome (middle), or tartrate resistant acid phosphatase (TRAP) with hematoxylin counterstain (right) of sham (top) or Myc-CaP injected mouse tibiae (bottom). (F) Osteoclast activity as measured by TRAcP-5b ELISA of peripheral blood plasma from sham injected or Myc-CaP intra-tibial tumor bearing animals. Data is presented as mean \pm SEM. * indicates $p < 0.05$.

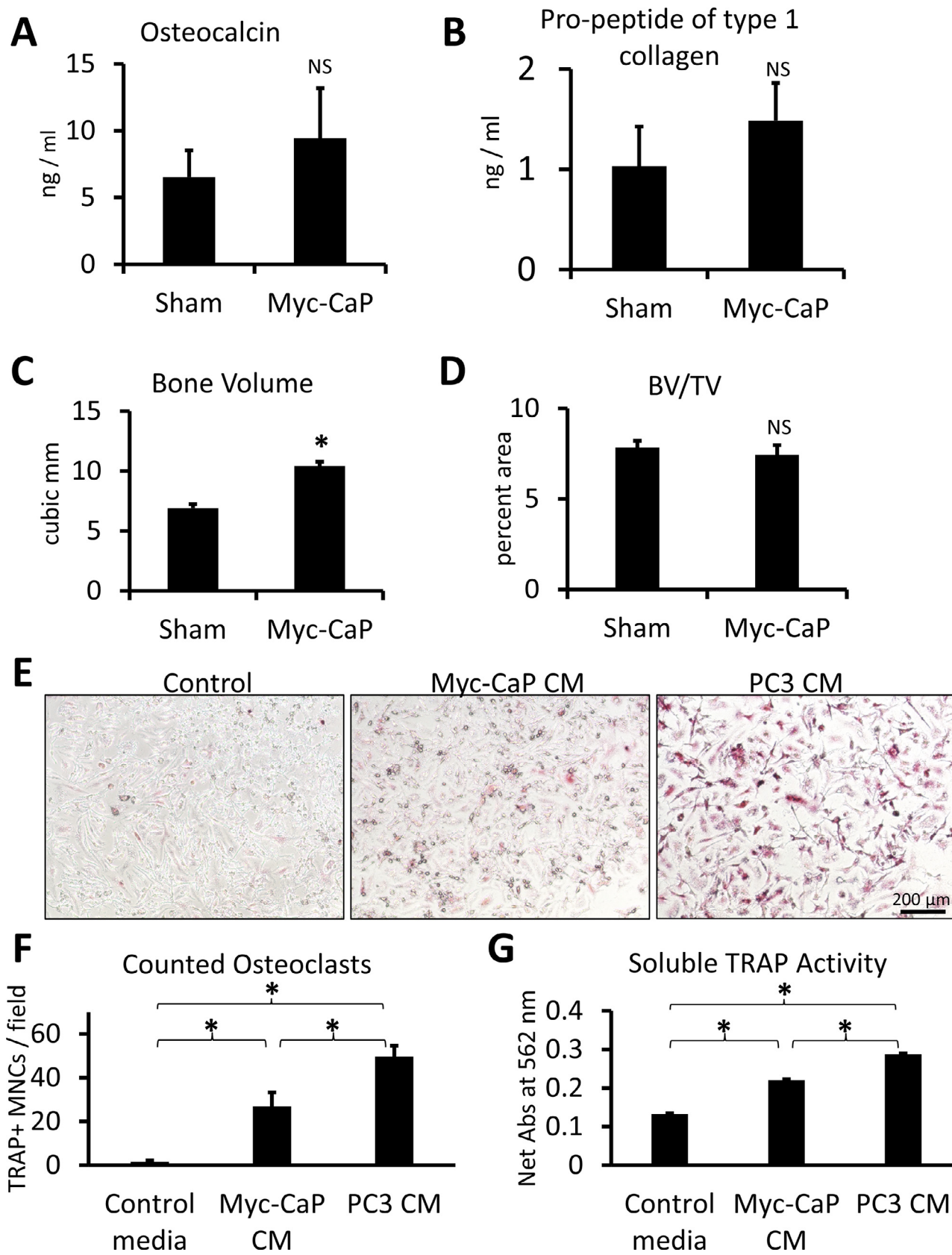


Fig. 3. Quantification of the Myc-CaP bone tumor phenotype. (A) and (B) Osteocalcin or type 1 collagen pro-peptide concentration in plasma of mice injected in the tibia with luciferase labeled Myc-CaP cells ($n = 14$) or PBS ($n = 4$). (C) and (D) Bone volume or the ratio of bone volume to total volume (BV/TV) in tibia injected with sham or luciferase Myc-CaP cells. (E) 100 × original magnification images of osteoclast cultures stained for TRAP (red). (F) TRAP + multinucleated cells per low power field of mouse OCL cultures with or without addition of conditioned media from Myc-CaP or PC3 cells. (G) Colorimetric assay of secreted TRAP activity in the mouse OCL cultures. Data is represented as mean ± SEM. * indicates $p < 0.05$. Data from *in vitro* studies represents quadruplicate wells from one of four independent experiments. (For interpretation of the references to colour in this figure legend, the reader is referred to the web version of this article.)

appeared to be in the mediastinum rather than arising from heart or lung. Histologically, the majority of the tumor volume was in the mediastinum, but we did observe small tumors in lung parenchyma as well (Fig. 1D). To further validate the distribution of metastases in the left cardiac ventricle injection model, we labeled Myc-CaP cells with tdTomato for *in vivo* imaging and isolation and performed left cardiac ventricle injections. Gross analysis, as aided by *ex vivo* fluorescent imaging, showed tumor cells in the bone; with putative tumor cells defined as tdTomato positive and negative for Ter119 (erythroid marker) and Cd45 (leukocyte marker) (Fig. 1F). We consistently found in excess of an order of magnitude more events in the tumor cell gate in Myc-CaP injected animals as compared to PBS injected controls.

To explore the potential of Myc-CaP cells as a bone metastasis model and to quantify the bone phenotype, we next examined their growth after intra-tibial intraosseous injection. To increase the sensitivity of *in vivo* imaging, we labeled the Myc-CaP cells with luciferase (Fig. 2A) before performing intra-tibial injections of Myc-CaP cells (14 FVB/NJ mice) or sham injections of PBS into 4 mice. These animals required euthanasia for limping, not using the affected hind limb, or tumor diameter >1 cm after about two months and had large tibial tumors at the time of necropsy (Fig. 2B). All 14 Myc-CaP injected mice developed grossly visible tumors. Tumor growth as measured by bioluminescence was detectable 5 days after injection and was only detectable in the left legs of Myc-CaP injected – but not sham injected animals (Fig. 2C). On micro computed tomography (μ -CT) analysis, the lesions had areas of both bone loss and apparent new bone formation including areas outside of the prior boundary of bone cortex (Fig. 2D). Because of the surprising finding of suspected extra-cortical bone formation, we analyzed the bones histologically. The extra-cortical bone areas stained as expected (pink) on hematoxylin and eosin (H&E) stains, and also as expected (blue) on Masson's tri-

chrome stain, which selectively stains collagen (Fig. 2E). Therefore, from the histologic findings and high attenuation on μ -CT analyses, we concluded that Myc-CaP bone tumors induce extra-osseous calcification in addition to abnormal bone formation within the existing bone cavity.

To further evaluate the presence of abnormal bone remodeling, we labeled sections from these specimens for tartrate resistant acid phosphatase (TRAP/Acp5), as a marker of mouse osteoclasts (OCLs) and observed increased TRAP staining of osteoclasts (OCLs) at many of the areas of extra-cortical ossification (Fig. 2E). However, we did not detect a difference in TRAP-5b in plasma from control compared to Myc-CaP tumor bearing animals (Fig. 2F).

To better determine if the Myc-CaP bone tumor phenotype is osteosclerotic, osteolytic, or mixed, we quantified bone remodeling parameters. The concentration of bone formation markers, osteocalcin and pro-peptide of type 1 collagen, trended higher in the plasma of mice injected with luciferase labeled Myc-CaP cells but was not statistically significant (Fig. 3A and 3B). Therefore, we quantified μ -CT images of the sham or Myc-CaP tumor bearing tibiae (Fig. 2D). Presence of the Myc-CaP tumor increased the bone volume in a statistically significant fashion (Fig. 3C). However, the ratio of the bone volume to total volume (BV/TV) remained unchanged (Fig. 3D). Therefore, we concluded that the volume of new bone induced by the tumors was approximately balanced by the increased bone area caused by extra-cortical ossification. To further assess the contribution of Myc-CaP cells to OCL formation, we assayed formation of OCLs *in vitro* from bone marrow of FVB/NJ mice. As assessed by microscopy, counted TRAP⁺ multi-nuclear cells, and activity of TRAP secreted into the media of the OCL cultures; conditioned media (CM) from Myc-CaP cells significantly induced OCL formation as compared to control media, but induced less OCL formation than the strongly osteolytic cell line, PC3 (Fig. 3E – 3G).

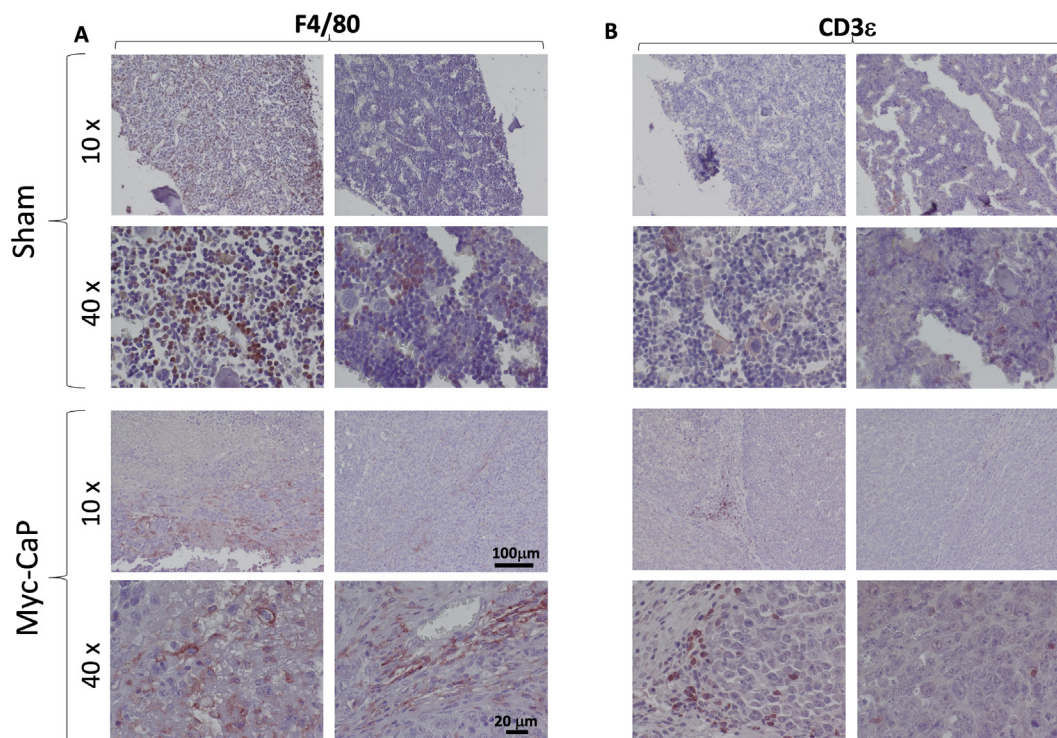


Fig. 4. Immune cell infiltration in Myc-CaP intra-tibial tumors. (A) IHC for macrophage marker, F4/80 (B) IHC for T-cell marker Cd3ε. Antigens are labeled in red. Nuclei are counter-stained with hematoxylin (blue). Two representative images acquired using either 10x or 40x objectives from either sham injected (top panels) or MycCaP tumor bearing animals (bottom panels) are shown for each condition as indicated. (For interpretation of the references to colour in this figure legend, the reader is referred to the web version of this article.)

Lastly, as an aid to researchers using this model in future studies of cancer immunity, we examined immune infiltration of luciferase labeled Myc-CaP tibial tumors. Upon immunohistochemistry (IHC) for F4/80, we observed a moderate macrophage infiltration, predominantly at the edge of the tumors (Fig. 4A). With the aid of labeling for Cd3ε, we observed a much more sparse T-cell infiltration, again predominantly at the periphery of the tumors (Fig. 4B). This low number of T-cells is in keeping with findings of multiple investigators that PCa is an immunologically “cold” tumor with low numbers of tumor infiltrating lymphocytes (TILs) [19]. Although various definitions and quantification methods have been used for TILs, CD3⁺ total T-cells and subsets, especially CD8⁺ T-cells are shown in other cancers to correlate with survival [20,21].

4. Discussion

Here we describe a new mouse model of PCa bone metastases, which shares important features of the disease of many metastatic prostate cancer patients. This model utilizes the Myc-CaP prostate cancer cell line inoculated into syngeneic FVB/NJ mice and therefore produces a model that requires androgen signaling and is immune competent. The FVB background Myc-CaP cell line models the most common type of deadly PCa; disease which initially responds to androgen deprivation, then becomes castration resistant (can grow in the presence of a low concentration of testosterone), but continues to require transcription regulated by the androgen receptor. Subcutaneous FVB Myc-CaP tumors established in intact FVB/NJ mice initially shrink after medical or surgical castration, but then uniformly progress within two months [22]. In patients, selective pressure of continual hormonal based therapies can induce the development of small cell neuroendocrine prostate cancer, or alternatively “double negative” prostate cancer which has neither androgen signaling nor neuroendocrine markers. However, even in modern patients, androgen receptor positive PCa remains the most common subtype of castration resistant disease [23]. One of the ways that prostate cancers become castration resistant while retaining androgen receptor related signaling is through ligand independent splice variants of the *AR* gene including *AR-v7*. FVB background Myc-CaP cells express splice variants of the *Ar* gene, whereas B6 background Myc-CaP cells do not [10]. This might explain why FVB Myc-CaP cells rapidly become castrate resistant *in vivo*, and in the current study, FVB Myc-CaP cells formed bone tumors after routine cell culture. But in another study using B6 background Myc-CaP cells, the investigators only observed bone tumor formation after preparing a single cell suspension of an existing tumor [15]. We expect the tumor growth from routine culture, which we present here, to expedite future mechanistic studies using FVB background Myc-CaP cells as a bone metastasis model.

Furthermore, because of the syngeneic and immune competent host, FVB Myc-CaP models are also well suited to studies of the immune system and immune therapy in prostate cancer [22]. This is unlike the more commonly used xenograft based models of metastatic PCa [6]. These studies are especially of interest because modern immune checkpoint inhibitors have not been effective enough in most PCa patients to garner approval from the U.S. F. D.A. or regulatory bodies in other countries, though many investigators are trying to understand the mechanisms of resistance. Prostate cancer tumors usually have a “cold” immune phenotype with scant numbers of tumor infiltrating lymphocytes, and induction of tolerance in many of the lymphocytes that are present [19]. In keeping with this literature, in this model we performed Cd3ε IHC of intra-tibial tumors and observed only rare infiltrating T-lymphocytes, predominantly near the edges of the tumors. Of

unique interest to PCa, androgens are reported to partially regulate tumor immunology, with androgen suppression favoring a more robust immune response [24]. Therefore, the previously reported ability of the FVB Myc-CaP model to respond to castration and later progress makes the model particularly attractive in studies of immunotherapy.

Lastly, development of a bone metastatic model of PCa is also notable because bone is the most common metastatic site for the disease. Indeed, 90% of patients who die of PCa have bone metastases [25]. Our studies showed that FVB Myc-CaP cells form bone metastases when administered both systemically (left ventricle intracardiac injection) and in a directed fashion when injected in the tibia. The results of our characterization of these tumors resembled the appearance of bone metastases in many PCa patients. We characterize the tumors as mixed osteosclerotic/osteolytic and quantitatively demonstrated new calcified bone formation, which curiously included areas outside of the prior cortical boundary. Although PCa bone metastases are predominantly osteosclerotic, mixed osteolytic/osteosclerotic PCa bone metastases, like our model, are not rare either and comprised 12.7% of patients in one series [26]. We also found that Myc-CaP conditioned media induced osteoclast formation *in vitro*, though not to the extent induced by the purely osteolytic cell line, PC3 [8]. While others have begun to use a femoral intraosseous injection adaptation of FVB Myc-CaP cells, there has been minimal description of the bone phenotype and no reports of bone metastases after systemic (intracardiac) administration as we describe here [12,13].

Useful further characterization of this model system could include which secreted factors are responsible for induction of osteoclast formation and new bone formation in this system. To begin these investigations, we measured the concentrations of soluble Trance (RANKL) and Cxcl15 (Il-8) in biologic triplicates of Myc-CaP conditioned media. However, the concentration of each was below the detection limit of the ELISA assays we used (<5 pg/mL for Rankl and 0.8 ng/mL for Il-8 – data not shown). However, we think that our demonstration of reliable bone tumor formation and characterization of the bone tumor phenotype will give investigators the necessary information to add this to their portfolio of PCa models. Overall, the FVB Myc-CaP model promises to be a clinically relevant and practical model of PCa bone metastases.

5. Conclusions

In these studies, we found that androgen receptor positive, murine FVB Myc-CaP cells form bone metastases in syngeneic FVB/NJ hosts with a mixed osteolytic/osteosclerotic appearance after systemic and localized intraosseous injection of cells cultured *in vitro*. The model therefore promises great utility for prostate cancer research involving bone, androgen signaling, or the immune system.

Funding

Direct funding was provided by the University of Michigan Prostate Cancer S.P.O.R.E. NIH/NCI 5 P50CA18678605, PI Arul Chinaiyan, Career Enhancement sub-award to F.C.C. F048931, and NIH/NCI P01-CA093900. F.C.C. and R.S.T. received support from The Prostate Cancer Foundation Challenge award 16CHAL05. R.T. received support as the Major McKinley Ash Colligate Professor at The University of Michigan. F.C.C. received support from The Prostate Cancer Foundation Young Investigator Award 18YOUN04, Department of Defense Prostate Cancer Research Program Physician Research Award W81XWH2010394, and start-up funds from The University of Michigan and Karmanos Cancer Institute. I.P. was funded by NIH/NCI R01 CA251394.

CRediT authorship contribution statement

Yu Wang: Investigation, Visualization, Methodology, Writing - review & editing. **Mackenzie K. Herroon:** Investigation, Visualization, Methodology, Writing - review & editing. **Steven P. Zielske:** Investigation, Visualization, Writing - review & editing. **Leigh Ellis:** Conceptualization, Methodology, Resources, Writing - review & editing. **Izabela Podgorski:** Investigation, Visualization, Methodology, Supervision, Writing - review & editing. **Russell S. Taichman:** Conceptualization, Supervision, Funding acquisition, Writing - review & editing. **Frank C. Cackowski:** Conceptualization, Supervision, Investigation, Visualization, Methodology, Funding acquisition, Writing - original draft, Writing - review & editing.

Declaration of Competing Interest

The authors declare that they have no known competing financial interests or personal relationships that could have appeared to influence the work reported in this paper.

Acknowledgements

The authors wish to thank Christopher Strayhorn of the University of Michigan School of Dentistry Histology Core for tissue processing, sectioning, and H&E and trichrome staining. We also thank Michelle Lynch of the University of Michigan School of Dentistry micro CT Core, funded in part by NIH/NCRR S10RR026475-01, for CT analyses.

References

- [1] SEER Cancer Statistics Factsheets: Prostate Cancer. National Cancer Institute. Bethesda, MD. December 9, 2016; Available from: <https://seer.cancer.gov/statfacts/html/prost.html>.
- [2] M.M. Grabowska et al., Mouse models of prostate cancer: picking the best model for the question, *Cancer Metastasis Rev.* 33 (2–3) (2014) 377–397.
- [3] A.A. Hurwitz et al., The TRAMP mouse as a model for prostate cancer, *Curr. Protoc. Immunol.* (2001), Chapter 20: p. Unit 20 5.
- [4] L.A. Kido, C. de Almeida Lamas, M.R. Maróstica, V.H.A. Cagnon, Transgenic Adenocarcinoma of the Mouse Prostate (TRAMP) model: A good alternative to study PCa progression and chemoprevention approaches, *Life Sci.* 217 (2019) 141–147.
- [5] X. Ma, A.C. Ziel-van der Made, B. Autar, H.A. van der Korput, M. Vermeij, P. van Duijn, K.B. Cleutjens, R. de Krijger, P. Krimpenfort, A. Berns, T.H. van der Kwast, J. Trapman, Targeted biallelic inactivation of Pten in the mouse prostate leads to prostate cancer accompanied by increased epithelial cell proliferation but not by reduced apoptosis, *Cancer Res.* 65 (13) (2005) 5730–5739.
- [6] S.H. Park, M.R. Eber, Y. Shiozawa, Models of Prostate Cancer Bone Metastasis, *Methods Mol. Biol.* 1914 (2019) 295–308.
- [7] A.M. Havens, E.A. Pedersen, Y. Shiozawa, C. Ying, Y. Jung, Y. Sun, C. Neeley, J. Wang, R. Mehra, E.T. Keller, L. K. McCauley, R.D. Loberg, K.J. Pienta, R.S. Taichman, An in vivo mouse model for human prostate cancer metastasis, *Neoplasia* 10 (4) (2008) 371–IN4.
- [8] A. Fradet et al., A new murine model of osteoblastic/osteolytic lesions from human androgen-resistant prostate cancer, *PLoS One* 8 (9) (2013) e75092.
- [9] P.A. Watson, K. Ellwood-Yen, J.C. King, J. Wongvipat, M.M. LeBeau, C.L. Sawyers, Context-dependent hormone-refractory progression revealed through characterization of a novel murine prostate cancer cell line, *Cancer Res.* 65 (24) (2005) 11565–11571.
- [10] L. Ellis, ShengYu Ku, Q. Li, G. Azabdafdari, J. Seliski, B. Olson, C.S. Netherby, D.G. Tang, S.I. Abrams, D.W. Goodrich, R. Pili, Generation of a C57BL/6 MYC-Driven Mouse Model and Cell Line of Prostate Cancer, *Prostate* 76 (13) (2016) 1192–1202.
- [11] S.O. Dudzinski et al., Combination immunotherapy and radiotherapy causes an abscopal treatment response in a mouse model of castration resistant prostate cancer, *J. Immunother. Cancer* 7 (1) (2019) 218.
- [12] S. Jiao et al., Differences in Tumor Microenvironment Dictate T Helper Lineage Polarization and Response to Immune Checkpoint Therapy, *Cell* 179 (5) (2019) 1177–1190 e13.
- [13] I. Vardaki et al., Radium-223 Treatment Increases Immune Checkpoint Expression in Extracellular Vesicles from the Metastatic Prostate Cancer Bone Microenvironment, *Clin. Cancer Res.* (2021).
- [14] B.W. Simons et al., A hemi-spleen injection model of liver metastasis for prostate cancer, *Prostate* (2020).
- [15] B.W. Simons, V. Kothari, B. Benzon, K. Ghabili, R. Hughes, J.C. Zarif, A.E. Ross, P. J. Hurley, E.M. Schaeffer, A mouse model of prostate cancer bone metastasis in a syngeneic immunocompetent host, *Oncotarget* 10 (64) (2019) 6845–6854.
- [16] Y. Oba, H.O.Y. Chung, S.J. Choi, G.D. Roodman, Eosinophil chemotactic factor-L (ECF-L): a novel osteoclast stimulating factor, *J. Bone Miner Res.* 18 (7) (2003) 1332–1341.
- [17] F.C. Cackowski et al., Osteoclasts are important for bone angiogenesis, *Blood* 115 (1) (2010) 140–149.
- [18] F.C. Cackowski, M.R. Eber, J. Rhee, A.M. Decker, K. Yumoto, J.E. Berry, E. Lee, Y. Shiozawa, Y. Jung, J.A. Aguirre-Ghisso, R.S. Taichman, Mer Tyrosine Kinase Regulates Disseminated Prostate Cancer Cellular Dormancy, *J. Cell Biochem.* 118 (4) (2017) 891–902.
- [19] E.K. Fay, J.N. Graff, Immunotherapy in Prostate Cancer, *Cancers (Basel)* 12 (2020) 7.
- [20] J. Hao et al., Prognostic impact of tumor-infiltrating lymphocytes in high grade serous ovarian cancer: a systematic review and meta-analysis, *Ther. Adv. Med. Oncol.* 12 (2020), p. 1758835920967241.
- [21] B.A. Berele, Y. Cai, G. Yang, Prognostic Value of Tumor Infiltrating Lymphocytes in Nasopharyngeal Carcinoma Patients: Meta-Analysis, *Technol. Cancer Res. Treat.* 20 (2021).
- [22] Y.-C. Shen, A. Ghasemzadeh, C.M. Kochel, T.R. Nirschl, B.J. Francica, Z.A. Lopez-Bujanda, M.A. Carrera Haro, A. Tam, R.A. Anders, M.J. Selby, A.J. Korman, C.G. Drake, Combining intratumoral Treg depletion with androgen deprivation therapy (ADT): preclinical activity in the Myc-CaP model, *Prostate Cancer Prostatic Dis.* 21 (1) (2018) 113–125.
- [23] M.P. Labrecque et al., Molecular profiling stratifies diverse phenotypes of treatment-refractory metastatic castration-resistant prostate cancer, *J. Clin. Invest.* 129 (10) (2019) 4492–4505.
- [24] J.N. Graff et al., A phase II single-arm study of pembrolizumab with enzalutamide in men with metastatic castration-resistant prostate cancer progressing on enzalutamide alone, *J. Immunother. Cancer* 8 (2) (2020).
- [25] L. Bubendorf, A. Schöpfer, U. Wagner, H. Moch, N. Willi, T.C. Gasser, M.J. Mihatsch, Metastatic patterns of prostate cancer: an autopsy study of 1,589 patients, *Hum. Pathol.* 31 (5) (2000) 578–583.
- [26] J.C. Chevillet, D. Tindall, C. Boelter, R. Jenkins, C.M. Lohse, V.S. Pankratz, T.J. Sebo, B. Davis, M.L. Blute, Metastatic prostate carcinoma to bone: clinical and pathological features associated with cancer-specific survival, *Cancer* 95 (5) (2002) 1028–1036.